Arch Appl Mech (2008) 78: 379–392
DOI 10.1007/s00419-007-0158-5

ORIGINAL

O. Ozdemir Ozgumus · M. O. Kaya

Flapwise bending vibration analysis of a rotating double-tapered Timoshenko beam

Received: 22 January 2007 / Accepted: 23 June 2007 / Published online: 11 September 2007

Abstract In this study, free vibration analysis of a rotating, double-tapered Timoshenko beam that undergoes flapwise bending vibration is performed. At the beginning of the study, the kinetic- and potential energy expressions of this beam model are derived using several explanatory tables and figures. In the following section, Hamilton's principle is applied to the derived energy expressions to obtain the governing differential equations of motion and the boundary conditions. The parameters for the hub radius, rotational speed, shear deformation, slenderness ratio, and taper ratios are incorporated into the equations of motion. In the solution, an efficient mathematical technique, called the differential transform method (DTM), is used to solve the governing differential equations of motion. Using the computer package Mathematica the effects of the incorporated parameters on the natural frequencies are investigated and the results are tabulated in several tables and graphics.

Keywords Nonuniform Timoshenko beam · Tapered Timoshenko beam · Rotating Timoshenko beam · Differential transform method · Differential transformation

List of symbols

A	cross-sectional area
b_0	beam breadth at the root section
c_b	breadth taper ratio
c_h	height taper ratio
E	Young's modulus
EA	axial rigidity of the beam cross section
EI	bending rigidity of the beam cross section
G	shear modulus
h_0	beam height at the root section
$\vec{i}, \vec{j}, \vec{k}$	unit vectors in the x, y, and z directions
I_y	second moment of inertia about the y axis
k	shear correction factor
kAG	shear rigidity
L	beam length
P	reference point after deformation
P_0	reference point before deformation

O. Ozdemir Ozgumus · M. O. Kaya (✉)
Istanbul Technical University, Faculty of Aeronautics and Astronautics, 34469 Maslak, Istanbul, Turkey
E-mail: kayam@itu.edu.tr
Tel: +90-212-2853110
Fax: +90-212-2852926

r	inverse of the slenderness ratio S
$\vec{r}_0$	position vector of P_0
$\vec{r}_1$	position vector of P
R	hub radius
S	slenderness ratio
t	time
T	centrifugal force
u_0	axial displacement due to the centrifugal force
U_b	potential energy due to bending
U_s	potential energy due to shear
V_x, V_y, V_z	velocity components of point P
$W[k]$, $\theta[k]$	transformed functions
w	flapwise bending displacement
w'	flapwise bending slope
x	spanwise coordinate
$\bar{x}$	spanwise coordinate parameter
x_0, y_0, z_0	coordinates of P_0
x_1, y_1, z_1	coordinates of P
δ	hub radius parameter
γ	shear angle
ε_0	uniform strain due to the centrifugal force
ε_{ij}	classical strain tensor
ε_{xx}	axial strain
$\varepsilon_{\eta\eta}$, $\varepsilon_{\xi\xi}$	transverse normal strains
η	sectional coordinate corresponding to major principal axis for P_0 on the elastic axis
μ	natural frequency parameter
ξ	sectional coordinate for P_0 normal to η axis at the elastic axis
ρ	density of the blade material
ρA	mass per unit length
θ	rotation angle due to bending
ω	circular natural frequency
Ω	constant rotational speed
$\bar{\Omega}$	rotational speed parameter

1 Introduction

The dynamic characteristics, i.e., natural frequencies and related mode shapes, of rotating tapered beams are required to determine resonant responses and perform forced vibration analysis. Therefore, many investigators have studied rotating tapered beams, which are very important for the design and performance evaluation of several engineering applications such as rotating machinery, helicopter blades, robot manipulators, spinning space structures, etc. Klein [11] used a combination of a finite-element approach and the Rayleigh–Ritz method to analyze the vibration of tapered beams. Downs [4] applied a dynamic discretization technique to calculate the natural frequencies of a nonrotating double-tapered beam based on both the Euler–Bernoulli and Timoshenko beam theories. Swaminathan and Rao [21], computed the frequencies of a pretwisted, tapered rotating blade using the Rayleigh–Ritz method and including the effects of the rotational speed, pretwist angle, and breadth taper. To [22] developed a higher-order tapered beam finite-element approach for transverse vibration of tapered cantilever beam structures. Sato [19] used the Ritz method to study a linearly tapered beam with ends constrained elastically against rotation and subjected to an axial force. Lau [12] studied the free vibrations of a tapered beam with an end mass using the exact method. Banerjee and Williams [2] derived the exact dynamic stiffness matrices of axial, torsional, and transverse vibrations for a range of tapered beam elements. Williams and Banerjee [23] studied the free vibration of an axially loaded beam with linear or parabolic taper, using a stepped approximation to model the beam as a rigidly connected set of uniform members. Storti and Aboelnaga [20] studied the transverse deflections of a straight tapered symmetric beam attached to a rotating hub as a model for the bending vibration of blades in turbomachinery. Kim and Dickinson [10] used the Rayleigh–Ritz

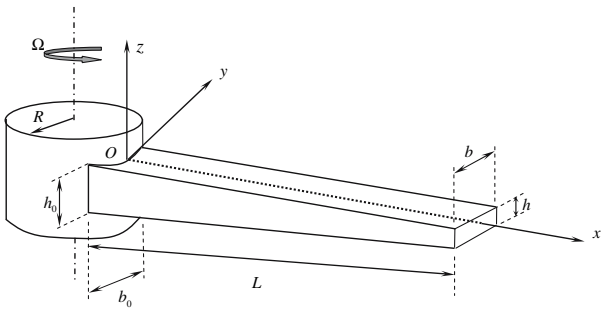

Fig. 1 Configuration of a rotating, double-tapered, cantilever Timoshenko beam

method to analyze slender beams subject to various complicated effects. Lee et al. [15] used the Green's function method in the Laplace transform domain to study the vibration of general elastically constrained tapered beams and obtained the approximate fundamental solution by using a number of stepped beams to represent the tapered beam. Lee and Kuo [13] used the Green's function method to study truncated nonuniform beams on an elastic base with polynomially varying bending rigidity and elastically constrained ends, giving an exact fundamental solution in power series form. Grossi and Bhat [6] used, respectively, the Rayleigh–Ritz method and the Rayleigh–Schmidt method to analyze the truncated tapered beams with rotational constraints at two ends. Naguleswaran [16] used the Frobenius method to analyze the free vibration of wedge and cone beams and beams with one constant side and another square-root-varying side. Bazoune and Khulief [3] developed a finite beam element for vibration analysis of a rotating double-tapered Timoshenko beam. Khulief and Bazoune [9] extended the work in Bazoune and Khulief [3] to account for different combinations of the fixed, hinged, and free end conditions.

In this study, as an extension of the authors' previous works [8,17,18], free vibration analysis of a rotating, double-tapered, cantilever Timoshenko beam that undergoes flapwise bending vibration is performed using the differential transform method (DTM), which is an iterative procedure to obtain analytic Taylor series solutions of differential equations. The advantage of DTM is its simplicity and accuracy in calculating the natural frequencies and plotting the mode shapes, and also its wide area of application. In the literature, there are several studies that have used DTM to deal with linear and nonlinear initial value problems, eigenvalue problems, ordinary and partial differential equations, aeroelasticity problems, etc. A brief review of these studies is given by Ozdemir Ozgumus and Kaya [17].

2 Beam configuration

The governing partial differential equations of motion are derived for the flapwise bending vibration of a rotating, double-tapered, cantilever Timoshenko beam represented by Fig. 1.

Here, a cantilever beam of length L, fixed at point O to a rigid hub, is shown. The hub has radius R and rotates in a counterclockwise direction at a constant rotational speed of Ω. The beam tapers linearly from a height of h_0 at the root to h at the free end in the xz plane and from a breadth b_0 to b in the xy plane. In the right-handed Cartesian coordinate system, the x-axis coincides with the neutral axis of the beam in the undeflected position, the z-axis is parallel to the axis of rotation (but not coincident), and the y-axis lies in the plane of rotation.

The following assumptions are made in this study,

a. The flapwise bending displacement is small.
b. The planar cross sections that are initially perpendicular to the neutral axis of the beam remain plane, but are no longer perpendicular to the neutral axis during bending.
c. The beam material is homogeneous and isotropic.

3 Derivation of the governing equations of motion

The cross-sectional and side views of the flapwise bending displacement of a rotating Timoshenko beam are shown in Fig. 2a and b, respectively.

Here, a reference point is chosen and is represented by P_0 before deformation and by P after deformation.

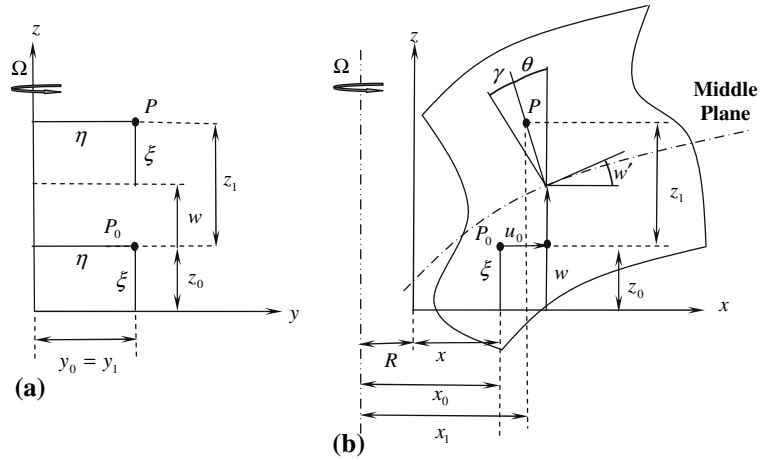

Fig. 2 **a** Cross-sectional view. **b** Longitudinal view of a rotating Timoshenko beam before and after flapwise bending deformation

3.1 Derivation of the potential energy expression

Examining Fig. 2a and b, the coordinates of the reference point are written as follows. Before deformation (coordinates of P_0):

$$x_0 = R + x, \quad y_0 = \eta, \quad z_0 = \xi. \tag{1}$$

After deformation (coordinates of P):

$$x_1 = R + x + u_0 - \xi\theta, \quad y_1 = \eta, \quad z_1 = w + \xi. \tag{2}$$

Here, the rotation angle due to bending, θ, is small, so it is assumed that $\mathrm{Sin}\theta \cong \theta$.

Knowing that $\vec{r}_0$ and $\vec{r}_1$ are the position vectors of P_0 and P, respectively, $\mathrm{d}\vec{r}_0$ and $\mathrm{d}\vec{r}_1$ can be given by

$$\mathrm{d}\vec{r}_0 = (\mathrm{d}x_0)\vec{i} + (\mathrm{d}y_0)\vec{j} + (\mathrm{d}z_0)\vec{k} \quad \text{and} \quad \mathrm{d}\vec{r}_1 = (\mathrm{d}x_1)\vec{i} + (\mathrm{d}y_1)\vec{j} + (\mathrm{d}z_1)\vec{k}. \tag{3}$$

The components of $\mathrm{d}\vec{r}_0$ and $\mathrm{d}\vec{r}_1$ are expressed as follows

$$\mathrm{d}x_0 = \mathrm{d}x, \quad \mathrm{d}y_0 = \mathrm{d}\eta, \quad \mathrm{d}z_0 = \mathrm{d}\xi \tag{4}$$

$$\mathrm{d}x_1 = (1 + u_0' - \xi\theta')\mathrm{d}x - \theta\mathrm{d}\xi, \quad \mathrm{d}y_1 = \mathrm{d}\eta, \quad \mathrm{d}z_1 = w'\mathrm{d}x + \mathrm{d}\xi \tag{5}$$

where the prime denotes differentiation with respect to the spanwise position x.

The classical strain tensor ε_{ij} may be obtained using the equilibrium equation below [5].

$$\mathrm{d}\vec{r}_1 \cdot \mathrm{d}\vec{r}_1 - \mathrm{d}\vec{r}_0 \cdot \mathrm{d}\vec{r}_0 = 2\lfloor \mathrm{d}x\mathrm{d}\eta\mathrm{d}\xi \rfloor \left[\varepsilon_{\mathrm{ij}}\right] \lfloor \mathrm{d}x\mathrm{d}\eta\mathrm{d}\xi \rfloor^{\mathrm{T}}. \tag{6}$$

Substituting Eqs. (4) and (5) into Eq. (6), the elements of the strain tensor ε_{ij} are obtained as follows

$$\varepsilon_{xx} = u_0' - \xi\theta' + \frac{\left(u'\right)^2}{2} + \frac{\xi^2\left(\theta'\right)^2}{2} - u_0'\theta'\xi + \frac{w'^2}{2}, \quad \gamma_{x\eta} = 0, \quad \gamma_{x\xi} = \left(w' - \theta\right) + \xi\theta\theta' - u_0'\theta. \tag{7}$$

In this work ε_{xx}, $\gamma_{x\eta}$, and $\gamma_{x\xi}$ are used in the calculations because, as noted by Hodges and Dowell [7], for long slender beams, the axial strain ε_{xx} is dominant over the transverse normal strains, $\varepsilon_{\eta\eta}$ and $\varepsilon_{\xi\xi}$. Moreover, the shear strain $\gamma_{\eta\xi}$ is two orders of magnitude smaller than the other shear strains, $\gamma_{x\eta}$ and $\gamma_{x\xi}$. Therefore, $\varepsilon_{\eta\eta}$, $\varepsilon_{\xi\xi}$, and $\gamma_{\eta\xi}$ can be neglected.

To obtain simpler expressions for the strain components, higher-order terms should be neglected so an order-of-magnitude analysis is performed by using the ordering scheme taken from Hodges and Dowell [7] and introduced in Table 1.

Table 1 Ordering scheme for Timoshenko beam formulation

$\frac{x}{L} = \mathrm{O}(1)$	$\frac{\eta}{L} = \mathrm{O}(\varepsilon)$
$\frac{w}{L} = \mathrm{O}(\varepsilon)$	$\theta = \mathrm{O}(\varepsilon)$
$\frac{\xi}{L} = \mathrm{O}(\varepsilon)$	$\frac{u_0}{L} = \mathrm{O}(\varepsilon^2)$
$\gamma = w' - \theta = \mathrm{O}(\varepsilon^2)$	

Table 2 Area integrals for the potential energy expression

$\iint\limits_A \mathrm{d}\eta\mathrm{d}\xi = A$	$\iint\limits_A \eta^2\,\mathrm{d}\eta\mathrm{d}\xi = I_z$	$\iint\limits_A \xi^2\,\mathrm{d}\eta\mathrm{d}\xi = I_y$
$\iint\limits_A \left(\eta^2 + \xi^2\right)\mathrm{d}\eta\mathrm{d}\xi = J$	$\iint\limits_A \xi\,\mathrm{d}\eta\mathrm{d}\xi = \iint\limits_A \eta\,\mathrm{d}\eta\mathrm{d}\xi = \iint\limits_A \xi\,\eta\,\mathrm{d}\eta\mathrm{d}\xi = 0$	

The Euler–Bernoulli beam theory is used by Hodges and Dowell [7]. In the present work, their formulation is modified for a Timoshenko beam and the following new expression is added to their ordering scheme as a contribution to the literature.

$$\gamma = w' - \theta = \mathrm{O}(\varepsilon^2). \tag{8}$$

Using Table 1, the strain components in Eq. (7) can be reduced to

$$\varepsilon_{xx} = u_0' - \xi\theta' + \frac{(w')^2}{2}, \quad \gamma_{x\eta} = 0, \quad \gamma_{x\xi} = w' - \theta. \tag{9}$$

Using Eq. (9), the potential energy expressions are derived. The potential energy contribution due to flapwise bending, U_b, is given by

$$U_\mathrm{b} = \frac{1}{2}\int\limits_0^L \left(\iint\limits_A E\varepsilon_{xx}^2\mathrm{d}\eta\mathrm{d}\xi\right)\mathrm{d}x. \tag{10}$$

Substituting the first expression of Eq. (9) into Eq. (10), taking integration over the blade cross section and referring to the definitions given by Table 2, the following potential energy expression is obtained for flapwise bending

$$U_\mathrm{b} = \frac{1}{2}\int\limits_0^L EA(u_0')^2\mathrm{d}x + \frac{1}{2}\int\limits_0^L EI_y(\theta')^2\mathrm{d}x + \frac{1}{2}\int\limits_0^L EAu_0'(w')^2\mathrm{d}x. \tag{11}$$

The uniform strain, ε_o, and the associated axial displacement, u_0, that is a result of the centrifugal force, $T(x)$, are related to each other as follows

$$u_0'(x) = \varepsilon_0(x) = \frac{T(x)}{EA} \tag{12}$$

where the centrifugal force is given by

$$T(x) = \int\limits_x^L \rho A\Omega^2(R + x)\mathrm{d}x. \tag{13}$$

Substituting Eq. (12) into Eq. (11) and noting that the $\frac{1}{2}\int_0^L \frac{T^2(x)}{EA}\mathrm{d}x$ term is constant and will be denoted as C_1, the final form of the bending potential energy is obtained as follows

$$U_\mathrm{b} = \frac{1}{2}\int\limits_0^L EI(\theta')^2\mathrm{d}x + \frac{1}{2}\int_0^L T(w')^2\mathrm{d}x + C_1. \tag{14}$$

The potential energy contribution due to shear, U_s, is given by

$$U_s = \frac{1}{2}\int_0^L \left[\iint_A \left(kG\gamma_{x\xi}^2\right) d\eta d\xi \right] dx. \tag{15}$$

Substituting the third expression of Eq. (9) into Eq. (15) and referring to the definitions given by Table 2, the following potential energy expression is obtained for the shear

$$U_s = \frac{1}{2}\int_0^L kAG(w' - \theta)^2 dx. \tag{16}$$

Summing Eqs. (14) and (16), the total potential energy expression is obtained

$$U = \frac{1}{2}\int_0^L \left[EI(\theta')^2 + kAG(w' - \theta)^2 + T(w')^2\right] dx + C_1. \tag{17}$$

3.2 Derivation of the kinetic energy expression

The velocity vector of the reference point P due to rotation of the beam is expressed as

$$\vec{V} = \frac{\partial \vec{r}_1}{\partial t} + \Omega \vec{k} \times \vec{r}_1. \tag{18}$$

Substituting the coordinates given by Eq. (2) into Eq. (18), the velocity components are obtained as follows

$$V_x = -\xi\dot{\theta} - \eta\Omega, \quad V_y = (R + x + u_0 - \xi\theta)\Omega, \quad V_z = \dot{w}. \tag{19}$$

Using Eq. (19), the kinetic energy expression, $\Im$, is derived as

$$\Im = \frac{1}{2}\int_0^L \left(\iint_A \rho\left(V_x^2 + V_y^2 + V_z^2\right) d\eta d\xi \right) dx. \tag{20}$$

Substituting Eq. (19) into Eq. (20) and referring to the definitions given by Table 3, the final form of the kinetic energy expression is obtained.

$$\Im = \frac{1}{2}\int_0^L \left(\rho A\dot{w}^2 + \rho I_y\dot{\theta}^2 + \rho I_y\Omega^2\theta^2\right) dx + C_2 \tag{21}$$

where C_2 includes the constant terms $\rho A(R + x + u_0)$ and $\rho I_z\Omega^2$ that appear after substituting Eq. (19) into Eq. (20).

Table 3 Area integrals for the kinetic energy expression

$\iint_A \rho\, d\eta d\xi = m$	$\iint_A \rho\, \eta^2\, d\eta d\xi = \rho\, I_z$	$\iint_A \rho\, \xi^2\, d\eta d\xi = \rho\, I_y$
$\iint_A \xi\, d\eta d\xi = \iint_A \eta\, d\eta d\xi = \iint_A \xi\, \eta\, d\eta d\xi = 0$		

3.3 Application of Hamilton's principle

The governing equations of motion and the associated boundary conditions can be derived by means of the Hamilton's principle, which can be stated in the following form for an undamped free vibration analysis.

$$\int_{t_1}^{t_2} \delta(U - \Im)\mathrm{d}t = 0. \tag{22}$$

Using variational principles, the variation of the kinetic and potential energy expressions are taken and the governing equations of motions of a rotating, nonuniform Timoshenko beam undergoing flapwise bending vibration are derived as follows

$$-\rho A\frac{\partial^2 w}{\partial t^2} + \frac{\partial}{\partial x}\left(T\frac{\partial w}{\partial x}\right) + \frac{\partial}{\partial x}\left[kAG\left(\frac{\partial w}{\partial x} - \theta\right)\right] = 0 \tag{23a}$$

$$-\rho I_y\frac{\partial^2 \theta}{\partial t^2} + \rho I_y\Omega^2\theta + \frac{\partial}{\partial x}\left(EI_y\frac{\partial \theta}{\partial x}\right) + kAG\left(\frac{\partial w}{\partial x} - \theta\right) = 0. \tag{23b}$$

Additionally, after the application of the Hamilton's principle, the associated boundary conditions are obtained as follows

- The geometric boundary conditions at the fixed end, $x = 0$, of the Timoshenko beam,

$$w(0, t) = \theta(0, t) = 0. \tag{24a}$$

- The natural boundary conditions at the free end, $x = L$, of the Timoshenko beam,

$$\text{Shear force:} T\frac{\partial w}{\partial x} + kAG\left(\frac{\partial w}{\partial x} - \theta\right) = 0. \tag{24b}$$

$$\text{Bending moment:} EI_y\frac{\partial \theta}{\partial x} = 0. \tag{24c}$$

The boundary conditions expressed by Eqs. (24b)–(24c) can be simplified by noting that $T = 0$ at the free end, $x = L$.

$$\frac{\partial w}{\partial x} - \theta = 0 \tag{25a}$$

$$\frac{\partial \theta}{\partial x} = 0. \tag{25b}$$

4 Vibration analysis

4.1 Harmonic motion assumption

In order to investigate the free vibration of the beam model considered in this study, a sinusoidal variation of $w(x, t)$ and $\theta(x, t)$ with a circular natural frequency, ω, is assumed and the functions are approximated as

$$w(x, t) = \bar{w}(x)\mathrm{e}^{i\omega t} \quad \text{and} \quad \theta(x, t) = \bar{\theta}(x)\mathrm{e}^{i\omega t}. \tag{26}$$

Substituting Eq. (26) into Eqs. (23a) and (23b), the equations of motion are expressed as

$$\rho A\omega^2\bar{w} + \frac{\mathrm{d}}{\mathrm{d}x}\left(T\frac{\mathrm{d}\bar{w}}{\mathrm{d}x}\right) + \frac{\mathrm{d}}{\mathrm{d}x}\left[kAG\left(\frac{\mathrm{d}\bar{w}}{\mathrm{d}x} - \bar{\theta}\right)\right] = 0 \tag{27a}$$

$$\rho I_y\omega^2\bar{\theta} + \rho I_y\Omega^2\bar{\theta} + \frac{\mathrm{d}}{\mathrm{d}x}\left(EI_y\frac{\mathrm{d}\bar{\theta}}{\mathrm{d}x}\right) + kAG\left(\frac{\mathrm{d}\bar{w}}{\mathrm{d}x} - \bar{\theta}\right) = 0. \tag{27b}$$

4.2 Tapered beam formulation and dimensionless parameters

The basic equations for the breadth $b(x)$, the height $h(x)$, the cross-sectional area, $A(x)$ and the second moment of inertia, $I_y(x)$ of a beam that tapers in two planes are

$$b(x) = b_0\left(1 - c_\mathrm{b}\frac{x}{L}\right)^m \quad \text{and} \quad h(x) = h_0\left(1 - c_\mathrm{h}\frac{x}{L}\right)^n \tag{28a}$$

$$A(x) = A_0\left(1 - c_\mathrm{b}\frac{x}{L}\right)^m\left(1 - c_\mathrm{h}\frac{x}{L}\right)^n \quad \text{and} \quad I_y(x) = I_{y0}\left(1 - c_\mathrm{b}\frac{x}{L}\right)^m\left(1 - c_\mathrm{h}\frac{x}{L}\right)^{3n} \tag{28b}$$

where the breadth taper ratio, c_b and the height taper ratio, c_h are given by

$$c_\mathrm{b} = 1 - \frac{b}{b_0} \quad \text{and} \quad c_\mathrm{h} = 1 - \frac{h}{h_0}. \tag{29}$$

The values of the constants n and m depend on the type of taper. In this study, the values $n = 1$ and $m = 1$ are used to model a beam that tapers linearly in two planes. Since the Young's modulus E, the shear modulus G and the material density, ρ are assumed to be constant, the mass per unit length ρA, the flapwise bending rigidity EI_y and the shear rigidity kAG vary according to the Eqs. (28a) and (28b).

In order to make comparisons with the results in the literature, the following dimensionless parameters can be introduced.

$$\bar{x} = \frac{x}{L} \quad \delta = \frac{R}{L} \quad \tilde{w} = \frac{\bar{w}}{L} \quad \mu^2 = \frac{\rho A_0 L^4 \omega^2}{EI_{y0}} \quad \bar{\Omega}^2 = \frac{\rho A_0 L^4 \Omega^2}{EI_{y0}} \quad r^2 = \frac{1}{S^2} = \frac{I_{y0}}{A_0 L^2} \quad s^2 = \frac{EI_{y0}}{kA_0 GL^2}. \tag{30}$$

Substituting the tapered beam formulas and the dimensionless parameters into Eqs. (27a) and (27b), the following dimensionless equations of motion are obtained for the linear taper case ($m = 1, n = 1$).

$$\begin{aligned}
&\frac{\mathrm{d}}{\mathrm{d}\bar{x}}\left[\left(\frac{c_\mathrm{b}c_\mathrm{h}}{4} + \delta - \frac{1}{2}(c_\mathrm{b}\delta + c_\mathrm{h}\delta - 1) - \frac{1}{3}(c_\mathrm{b} + c_\mathrm{h}\delta - c_\mathrm{b}c_\mathrm{h}\delta) - \bar{x}\delta + \frac{\bar{x}^2}{2}(c_\mathrm{b}\delta + c_\mathrm{h}\delta - 1)\right.\right.\\
&\left.\left. + \frac{\bar{x}^3}{3}(c_\mathrm{b} + c_\mathrm{h}\delta - c_\mathrm{b}c_\mathrm{h}\delta) - \frac{\bar{x}^4}{4}c_\mathrm{b}c_\mathrm{h}\right)\frac{\mathrm{d}\tilde{w}}{\mathrm{d}\bar{x}}\right] + \left(\frac{\mu}{\bar{\Omega}}\right)^2(1 - c_\mathrm{b}\bar{x})(1 - c_\mathrm{h}\bar{x})\tilde{w}\\
&+\left(\frac{1}{s\bar{\Omega}}\right)^2\frac{\mathrm{d}}{\mathrm{d}\bar{x}}\left[(1 - c_\mathrm{b}\bar{x})(1 - c_\mathrm{h}\bar{x})\left(\frac{\mathrm{d}\tilde{w}}{\mathrm{d}\bar{x}} - \bar{\theta}\right)\right] = 0
\end{aligned} \tag{31a}$$

$$\begin{aligned}
&\frac{\mathrm{d}}{\mathrm{d}\bar{x}}\left[(1 - c_\mathrm{b}\bar{x})(1 - c_\mathrm{h}\bar{x})^3\frac{\mathrm{d}\bar{\theta}}{\mathrm{d}\bar{x}}\right] + r^2\left(\mu^2 + \bar{\Omega}^2\right)(1 - c_\mathrm{b}\bar{x})(1 - c_\mathrm{h}\bar{x})^3\bar{\theta}\\
&+\frac{1}{s^2}(1 - c_\mathrm{b}\bar{x})(1 - c_\mathrm{h}\bar{x})\left(\frac{\mathrm{d}\tilde{w}}{\mathrm{d}\bar{x}} - \bar{\theta}\right) = 0.
\end{aligned} \tag{31b}$$

Additionally, substituting the dimensionless parameter into Eqs. (24a)–(25b), the dimensionless boundary conditions of a rotating cantilever Timoshenko beam can be obtained as

$$\text{At } \bar{x} = 0 \quad \tilde{w} = \bar{\theta} = 0 \tag{32a}$$

$$\text{At } \bar{x} = 1 \quad \frac{\mathrm{d}\tilde{w}}{\mathrm{d}\bar{x}} - \bar{\theta} = 0 \quad \text{and} \quad \frac{\mathrm{d}\bar{\theta}}{\mathrm{d}\bar{x}} = 0. \tag{32b}$$

5 The differential transform method

The differential transform method is a transformation technique based on the Taylor series expansion and is a useful tool to obtain analytical solutions of these differential equations. In this method, certain transformation rules are applied to both the governing differential equations of motion and the boundary conditions of the system in order to transform them into a set of algebraic equations. The solution of these algebraic equations gives the desired results of the problem. This approach is different from the high-order Taylor series method because the Taylor series method requires symbolic computation of the necessary derivatives of the data functions and is expensive for large orders. The details of the application procedure of DTM are explained by Ozdemir Ozgumus and Kaya [17] using several explanatory tables.

6 Formulation with DTM

In the solution step, DTM is applied to Eqs. (31a) and (31b) and the following expressions are obtained.

$$\begin{aligned}
&\left[\frac{1}{2}+\delta+\frac{1}{s^2\bar{\Omega}^2}-\frac{(2+3\delta)}{6}(c_\mathrm{b}+c_\mathrm{h})+\frac{(3+4\delta)}{12}c_\mathrm{b}c_\mathrm{h}\right](k+1)(k+2)W[k+2]\\
&-(k+1)^2\left(\delta+\frac{c_\mathrm{b}+c_\mathrm{h}}{s^2\bar{\Omega}^2}\right)W[k+1]+\left\{k(k+1)\left[\frac{(c_\mathrm{b}+c_\mathrm{h})\delta}{2}+\frac{c_\mathrm{b}c_\mathrm{h}}{s^2\bar{\Omega}^2}-\frac{1}{2}\right]+\frac{\mu^2}{\bar{\Omega}^2}\right\}W[k]\\
&+\left[\frac{(k-1)(k+1)}{3}(c_\mathrm{b}+c_\mathrm{h}+\delta c_\mathrm{b}c_\mathrm{h})-(c_\mathrm{b}+c_\mathrm{h})\frac{\mu^2}{\bar{\Omega}^2}\right]W[k-1] \qquad (33a)\\
&+\left[\frac{\mu^2}{\bar{\Omega}^2}-\frac{(k+1)(k+2)}{4}\right]c_\mathrm{b}c_\mathrm{h}W[k-2]-\frac{(k+1)}{s^2\bar{\Omega}^2}\theta[k+1]+\frac{c_\mathrm{b}+c_\mathrm{h}}{s^2\bar{\Omega}^2}(k+1)\theta[k]\\
&-\frac{c_\mathrm{b}c_\mathrm{h}}{s^2\bar{\Omega}^2}(k+1)\theta[k-1]=0\\
&(k+1)(k+2)\theta[k+2]-(c_\mathrm{b}+3c_\mathrm{h})(k+1)^2\theta[k+1]\\
&+[3c_\mathrm{h}(c_\mathrm{b}+c_\mathrm{h})k(k+1)-\frac{1}{s^2}+r^2\left(\mu^2+\bar{\Omega}^2\right)\Big]\theta[k]\\
&-\left[c_\mathrm{h}^2(k-1)(k+1)(3c_\mathrm{b}+c_\mathrm{h})-\frac{c_\mathrm{b}+c_\mathrm{h}}{s^2}+r^2\left(\mu^2+\bar{\Omega}^2\right)(c_\mathrm{b}+3c_\mathrm{h})\right]\theta[k-1]\\
&+\left[c_\mathrm{b}c_\mathrm{h}^3(k+1)(k-2)-\frac{c_\mathrm{b}c_\mathrm{h}}{s^2}+3c_\mathrm{h}(c_\mathrm{b}+c_\mathrm{h})r^2\left(\mu^2+\bar{\Omega}^2\right)\right]\theta[k-2] \qquad (33b)\\
&-\left[c_\mathrm{h}^2(3c_\mathrm{b}+c_\mathrm{h})r^2\left(\mu^2+\bar{\Omega}^2\right)\right]\theta[k-3]+c_\mathrm{b}c_\mathrm{h}^3r^2\left(\mu^2+\bar{\Omega}^2\right)\theta[k-4]\\
&+\frac{(k+1)}{s^2}W[k+1]-\frac{(c_\mathrm{b}+c_\mathrm{h})k}{s^2}W[k]+\frac{c_\mathrm{b}c_\mathrm{h}(k-1)}{s^2}W[k-1]=0.
\end{aligned}$$

Additionally, DTM is applied to Eqs. (32a)–(32b) and the following transformed boundary conditions are obtained.

$$\text{At } \bar{x}=0 \quad W[0]=\theta[0]=0 \qquad (34a)$$

$$\text{At } \bar{x}=1 \quad \sum_{k=0}^{\infty}(kW[k]-\theta[k])=0 \quad \text{and} \quad \sum_{k=0}^{\infty}k\theta[k]=0. \qquad (34b)$$

In Eqs. (33a)–(34b), $W[k]$ and $\theta[k]$ are the differential transforms of $\tilde{w}(\bar{x})$ and $\bar{\theta}(\bar{x})$, respectively. Using Eqs. (33a) and (33b), $W[k]$ and $\theta[k]$ values can now be evaluated in terms of $c_\mathrm{b}, c_\mathrm{h}, \mu, \bar{\Omega}, d_1$ and d_2 for $k=2,3\ldots$ The results calculated in Mathematica for $\delta=0$, $r=0.02$, $k=2/3$, and $E/G=8/3$ values are

$$\begin{aligned}
W[2]&=-3750\frac{d_2+(c_\mathrm{b}+c_\mathrm{h})d_1}{7500+(6-4c_\mathrm{h}-4c_\mathrm{b}+3c_\mathrm{h}c_\mathrm{b})\bar{\Omega}^2}\\
W[3]&=\frac{781250d_1-(1250.04c_\mathrm{b}+3750c_\mathrm{h})d_2+2499.96(c_\mathrm{b}+c_\mathrm{h})d_2}{7500+(6-4c_\mathrm{h}-4c_\mathrm{b}+3c_\mathrm{h}c_\mathrm{b})\bar{\Omega}^2}\\
&\quad+\frac{\left[2499.96c_\mathrm{h}c_\mathrm{b}+2.04\left(\mu^2-\bar{\Omega}^2\right)\right]d_1}{7500+(6-4c_\mathrm{h}-4c_\mathrm{b}+3c_\mathrm{h}c_\mathrm{b})\bar{\Omega}^2}-18750000\frac{[(c_\mathrm{b}+c_\mathrm{h})d_1+d_2](c_\mathrm{b}+c_\mathrm{h})}{\left[7500+(6-4c_\mathrm{h}-4c_\mathrm{b}+3c_\mathrm{h}c_\mathrm{b})\bar{\Omega}^2\right]^2}\\
\theta[2]&=-312.5d_1+0.5(c_\mathrm{b}+3c_\mathrm{h})d_2\\
\theta[3]&=104.17(c_\mathrm{b}+c_\mathrm{h})d_1-781250\frac{(c_\mathrm{b}+c_\mathrm{h})d_1+d_2}{7500+(6-4c_\mathrm{h}-4c_\mathrm{b}+3c_\mathrm{h}c_\mathrm{b})\bar{\Omega}^2}\\
&\quad+(0.33c_\mathrm{b}+c_\mathrm{h})[-625d_1+(c_\mathrm{b}+3c_\mathrm{h})d_2]-\left[-104.17+c_\mathrm{h}c_\mathrm{b}+c_h^2+0.000067\left(\bar{\Omega}^2+\mu^2\right)\right]d_2.
\end{aligned}$$

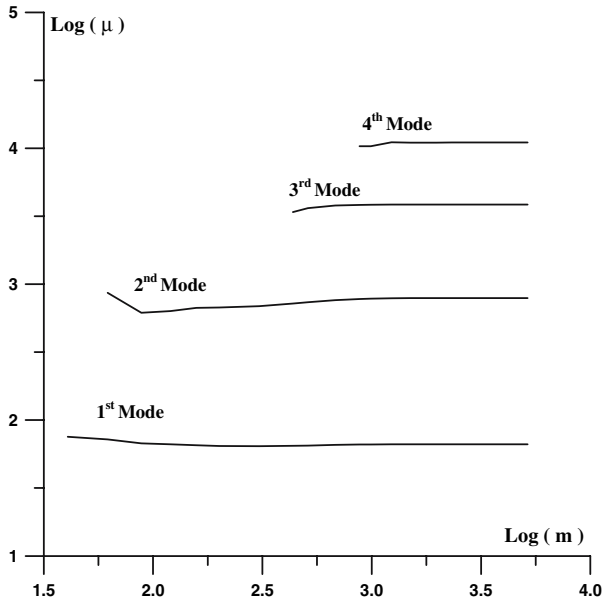

Fig. 3 Convergence of the first four natural frequencies ($\delta = 0$, $\overline{\Omega} = 4$, $c_b = c_h = 0.5$, $r = 0.08$, $v = 0.3$, $k = 0.85$)

Here the constants d_1 and d_2 that appear in the $W[k]$s and $\theta[k]$s are defined as follows

$$d_1 = W[1] = \left(\frac{\mathrm{d}\tilde{w}}{\mathrm{d}\bar{x}}\right)_{x=0} \quad \text{and} \quad d_2 = \theta[1] = \left(\frac{\mathrm{d}\theta}{\mathrm{d}\bar{x}}\right)_{x=0}. \tag{35}$$

7 Results and discussions

The computer package Mathematica is used to write code for the expressions given by Eqs. (33a)–(34b). The effects of the rotational speed, hub radius, slenderness ratio, and taper ratios on the natural frequencies are investigated and the related graphics are plotted. Additionally, in order to validate the calculated results, comparisons with the studies in the literature are made and very good agreement between the results is observed.

In Fig. 3, convergence of the first four natural frequencies with respect to the number of terms, used in the DTM application is introduced. In order to evaluate up to the fourth natural frequency with five-digit precision, it was necessary to include 39 terms. During the calculations, it was noticed that, when the rotational speed parameter was increased, the number of terms had to be increased to achieve the same accuracy. Additionally, here it was seen that higher modes appear when more terms were taken into account in application of the DTM. Thus, depending on the order of the required mode, one must try a few values for the number of terms at the beginning of the Mathematica calculations to find the adequate number of terms.

In Fig. 4, the variation of the first three natural frequencies of a rotating tapered Timoshenko beam with respect to the rotational speed parameter, $\bar{\Omega}$ and the hub radius parameter, δ, is shown. As expected, the natural frequencies increase with increasing rotational speed parameter due to the stiffening effect of the centrifugal force, which is directly proportional to the square of the rotational speed. Moreover, as seen in Fig. 4, δ makes the rate of increase of the natural frequencies larger because the centrifugal force, which is directly proportional to the hub radius, makes the beam stiffer for increasing δ (Fig. 4).

In Table 4, the variation of the natural frequencies of a uniform beam with respect to the inverse of the slenderness ratio, r, and the rotational speed parameter, $\bar{\Omega}$, is introduced and the results are compared with those given by Banerjee [1]. Besides increasing with the rotational speed parameter, the natural frequencies decrease as the inverse of the slenderness ratio, r, increases. At $\bar{\Omega} = 12$, the decrease in the frequencies due to r is 7% for the first mode, 23.12% for the second mode, 37% for the third mode, and 59.7% for the fourth mode. Comparing the percentage decrease in the frequencies, it is noticed that the effect of the slenderness ratio is dominant for the higher modes and this effect diminishes rapidly as the frequency order decreases. This is expected because the Timoshenko beam theory is used when the higher mode frequencies are of interest. The

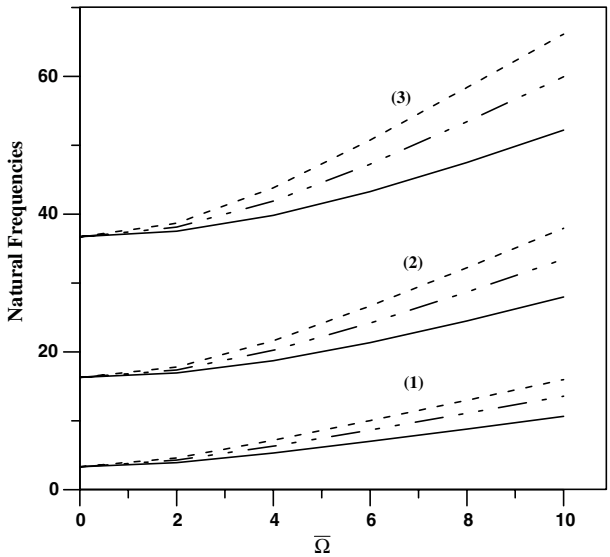

Fig. 4 Variation of the natural frequencies with respect to the hub radius parameter, δ and the rotational speed parameter, $\overline{\Omega}$ ($r = 0.08$, $v = 0.3$, $k = 0.5$, $\delta = 1$ dashed line; $\delta = 0.5$ dashed dotted line; $\delta = 0$ solid line)

Table 4 Variation of the natural frequencies of a uniform Timoshenko beam with respect to the inverse of the slenderness ratio parameter, r and rotational speed parameter, $\overline{\Omega}$ ($c_b = c_h = 0$, $k = 2/3$, $E/G = 8/3$, $\delta = 0$)

r	Natural frequencies							
	$\overline{\Omega}$							
	0		4		8		12	
	Present	Ref. [1]	Present	Ref. [1]	Present	Ref. [1]	Present	Ref. [1]
0	3.51601	3.5160	5.58500	5.585	9.25684	9.2568	13.1702	13.170
	22.0345	–	24.2733	–	29.9954	–	37.6031	–
	61.6971	–	63.9666	–	70.2929	–	79.6144	–
	120.901	–	123.261	–	130.049	–	140.534	–
0.02	3.49980	3.4998	5.56158	5.5616	9.20959	9.2096	13.0870	13.087
	21.3547	–	23.6061	–	29.3215	–	36.8659	–
	57.4705	–	59.8117	–	66.2748	–	75.6698	–
	106.926	–	109.459	–	116.665	–	127.604	–
0.04	3.45267	3.4527	5.49511	5.4951	9.08544	9.0854	12.8934	12.893
	19.6497	–	21.9557	–	27.7082	–	35.1811	–
	48.8891	–	51.4822	–	58.4507	–	68.2339	–
	84.1133	–	87.1836	–	95.6423	–	107.887	–
0.06	3.37873	3.3787	5.39542	5.3954	8.92085	8.9208	12.6724	12.672
	17.5470	–	19.9662	–	25.8362	–	33.2672	–
	40.7447	–	43.7365	–	51.4154	–	61.6011	–
	66.3623	–	70.1298	–	79.9414	–	93.0672	–
0.08	3.28370	3.2837	5.27486	5.2749	8.74555	8.7456	12.4581	12.458
	15.4883	–	18.0628	–	24.0479	–	31.2846	–
	34.3005	–	37.7317	–	45.9683	–	55.9744	–
	53.6516	–	57.9491	–	67.8215	–	77.1047	–
0.1	3.17377	3.1738	5.14482	5.1448	8.57351	8.5735	12.2467	12.247
	13.6607	–	16.3946	–	22.3506	–	28.9100	–
	29.3614	–	33.1793	–	41.4632	–	49.6484	–
	43.9102	–	47.8101	–	53.2833	–	56.6750	–

effect of the slenderness ratio can be observed better in Fig. 5, where the variation of the natural frequencies with respect to the inverse of the slenderness ratio, r, is shown.

In Table 5, the variation of the natural frequencies of a nonrotating Timoshenko beam with respect to various combinations of breadth and height taper ratios is given as a reference for the future studies and the results are compared with those calculated by Downs [4].

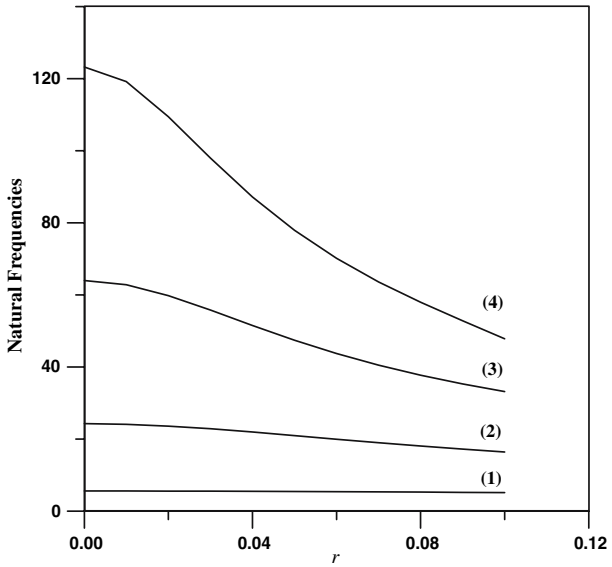

Fig. 5 Variation of the natural frequencies of a uniform rotating Timoshenko beam with respect to the inverse of the slenderness ratio effect, r ($\delta = 0$, $\overline{\Omega} = 4$, $k = 2/3$, $E/G = 8/3$, $c_b = c_h = 0$)

Table 5 Variation of the natural frequencies of a nonrotating Timoshenko beam with different combinations of breadth and height taper ratios ($r = 0.08$, $E/kG = 3.059$, $\delta = 0$)

c_h	c_b								
	0	0.1	0.2	0.3	0.4	0.5	0.6	0.7	0.8
0	3.32404	3.42876	3.5485	3.68722	3.85054	4.04668	4.28828	4.59598	5.00621
	3.32405[a]	–	–	3.68723[a]	–	–	4.28829[a]	–	5.00623[a]
	16.2889	16.4625	16.6561	16.8750	17.127	17.4242	17.7869	18.253	18.9024
	16.2890[a]	–	–	16.8752[a]	–	–	17.7871[a]	–	18.9026[a]
	36.7073	36.8384	36.9869	37.1583	37.3608	37.6076	37.9216	38.347	38.9849
	36.7078[a]	–	–	37.1588[a]	–	–	37.9221[a]	–	38.9854[a]
	58.2778	58.394	58.5281	58.6862	58.8777	59.1179	59.4326	59.8717	60.5467
	58.2788[a]	–	–	58.6872[a]	–	–	59.4336[a]	–	60.5477[a]
0.2	3.42466	3.52998	3.65042	3.78999	3.95437	4.15186	4.39529	4.70561	5.11985
	15.8905	16.0538	16.2362	16.4429	16.6816	16.9642	17.3110	17.7598	18.3917
	35.4301	35.5595	35.7054	35.8731	36.0704	36.3101	36.6141	37.0259	37.6454
	56.8910	57.0023	57.1293	57.2775	57.4552	57.6759	57.9630	58.3626	58.9813
0.4	3.56054	36.6661	3.78791	3.9285	4.09410	4.29314	4.5386	4.85176	5.27027
	15.3528	15.5057	15.6769	15.8715	16.0970	16.3651	16.6961	17.1278	17.7423
	33.7876	33.9159	34.0602	34.2253	34.4189	34.6531	34.9495	35.3502	35.9542
	54.7561	54.8654	54.9893	55.1324	55.3024	55.5115	55.7815	56.1557	56.7371
0.6	3.76227	3.86943	3.99193	4.13388	4.30106	4.50198	4.74978	5.06597	5.48870
	3.76228[a]	–	–	4.13389[a]	–	–	4.74979[a]	–	5.48871[a]
	14.6448	14.7872	14.9472	15.1296	15.3418	15.5954	15.9106	16.3251	16.9223
	14.6449[a]	–	–	15.1297[a]	–	–	15.9107[a]	–	16.9224[a]
	31.6239	31.7515	31.8945	32.0578	32.2486	32.4786	32.7688	33.1603	33.7509
	31.6243[a]	–	–	32.0582[a]	–	–	32.7693[a]	–	33.7513[a]
	51.6225	51.7327	51.8566	51.9987	52.1660	52.3699	52.6309	52.9901	53.5473
	51.6225[a]	–	–	51.9995[a]	–	–	52.6316[a]	–	53.5481[a]
0.8	4.11768	4.22692	4.35163	4.49590	4.66552	4.86899	5.11941	5.43815	5.86286
	13.7574	13.8888	14.0370	14.2068	14.4055	14.6445	14.9439	15.3418	15.9229
	28.6360	28.7620	28.9031	29.0641	29.2519	29.4779	29.7625	30.1461	30.7255
	46.8288	46.9419	47.0683	47.2125	47.3811	47.5848	47.8431	48.1956	48.7392

[a] Downs [4]

Furthermore, in order to observe the effects of the taper ratios, Fig. 6a and b can be considered. As seen in Fig. 6a and b, the breadth taper ratio, c_b, has very little or even no influence on the flapwise bending frequencies while the height taper ratio, c_h, has a linear decreasing effect on the natural frequencies except the fundamental natural frequency, which increases a little with c_h.

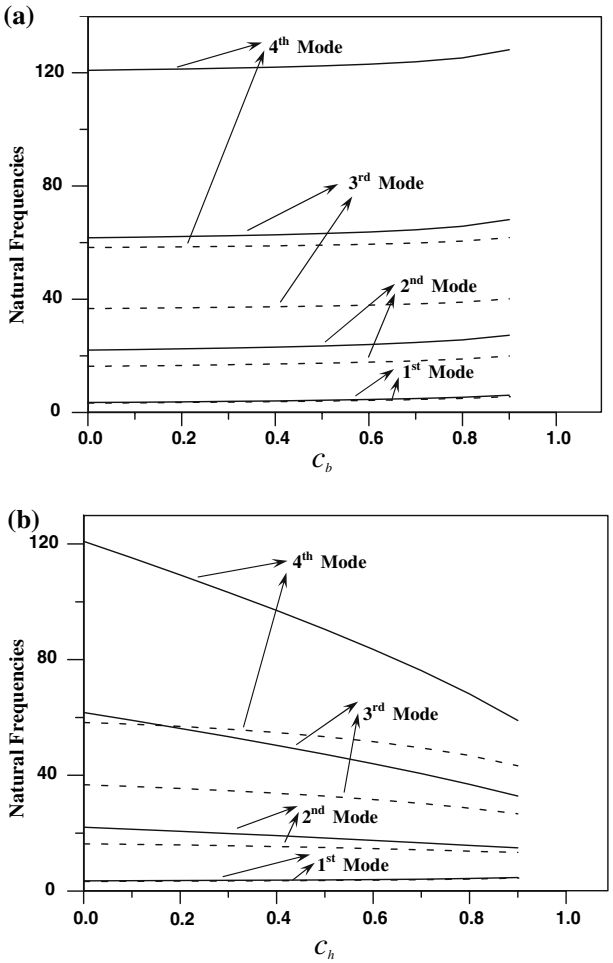

Fig. 6 Effects of the taper ratios, c_{b} and c_{h}, on the natural frequencies ($\delta = 0$, $\overline{\Omega} = 0$, $r = 0.08$, $v = 0.3$, $k = 0.85$). Euler: solid line; Timoshenko: dashed line

8 Conclusion

The main contributions of this study to the literature appear in the derivation of the governing equations of motion and can be summarized as follows:

- The detailed and clear derivation of both the potential and the kinetic energy expressions.
- In the study of Hodges and Dowell [7], the Euler–Bernoulli beam theory is used while in the present study their formulation is modified for the Timoshenko beam theory and a new expression, $\gamma = w' - \varphi = \mathrm{O}(\varepsilon^2)$, is added to their ordering scheme.

The effects of the slenderness ratio, hub radius, rotational speed and taper ratios on the natural frequencies are examined. The following results are obtained:

- The natural frequencies increase with the increasing rotational speed and this rate of increase becomes larger with increasing hub radius parameter, δ.
- The effect of the rotational speed is dominant on the fundamental natural frequency and this effect diminishes rapidly as the frequency order increases.
- The height taper ratio has a slight increasing effect on the fundamental natural frequency. The other natural frequencies decrease as the height taper ratio increases.
- The breadth taper ratio has very little, or even no influence, on the bending frequencies.
- The inverse of the slenderness ratio has a decreasing effect on the natural frequencies. Therefore, the natural frequencies of a Timoshenko beam are lower than the natural frequencies of a Euler–Bernoulli beam.

References

1. Banerjee, J.R.: Dynamic stiffness formulation and free vibration analysis of centrifugally stiffened Timoshenko beams. J. Sound Vib. **247**(1), 97–115 (2001)
2. Banerjee, J.R., Williams, F.W.: Exact Bernoulli–Euler dynamic stiffness matrix for a range of tapered beams. Int. J. Numer. Methods Eng. **21**, 2289–2302 (1985)
3. Bazoune, A., Khulief, Y.A.: A finite beam element for vibration analysis of rotating tapered Timoshenko beams. J. Sound Vib. **156**, 141–164 (1992)
4. Downs, B.: Transverse vibrations of cantilever beam having unequal breadth and depth tapers. ASME J. Appl. Mech. **44**, 737–742 (1977)
5. Eringen, A.C.: Mechanics of continua. Robert E. Krieger, Huntington (1980)
6. Grossi, R.O., Bhat, R.B.: A note on vibrating tapered beams. J. Sound Vib. **147**, 174–178 (1991)
7. Hodges, D.H., Dowell, E.H.: Nonlinear equations of motion for the elastic bending and torsion of twisted nonuniform rotor blades. NASA TN D-7818 (1974)
8. Kaya, M.O.: Free vibration analysis of rotating Timoshenko beams by differential transform method. Aircr. Eng. Aerosp. Tech. **78**(3), 194–203 (2006)
9. Khulief, Y.A., Bazoune, A.: Frequencies of rotating tapered Timoshenko beams with different boundary conditions. Comput. Struct. **42**, 781–795 (1992)
10. Kim, C.S., Dickinson, S.M.: On the analysis of laterally vibrating slender beams subject to various complicating effects. J. Sound Vib. **122**, 441–455 (1988)
11. Klein, L.: Transverse vibrations of non-uniform beam. J. Sound Vib. **37**, 491–505 (1974)
12. Lau, J.H.: Vibration frequencies of tapered bars with end mass. ASME J. Appl. Mech. **51**, 179–181 (1984)
13. Lee, S.Y., Kuo, Y.H.: Exact solution for the analysis of general elastically restrained non-uniform beams. ASME J. Appl. Mech. **59**, 205–212 (1992)
14. Lee, S.Y., Lin, S.M.: Bending vibrations of rotating non-uniform Timoshenko beams with an elastically restrained root. J. Appl. Mech. **61**, 949–955 (1994)
15. Lee, S.Y., Ke, H.Y., Kuo, Y.H.: Analysis of non-uniform beam vibration. J. Sound Vib. **142**, 15–29 (1990)
16. Naguleswaran, S.: Vibration in the two principal planes of a non-uniform beam of rectangular cross-section, one side of which varies as the square root of the axial co-ordinate. J. Sound Vib. **172**, 305–319 (1994)
17. Ozdemir Ozgumus, O., Kaya, M.O.: Flexural vibration analysis of double tapered rotating Euler–Bernoulli beam by using the differential transform method. Meccanica **41**(6), 661–670 (2006)
18. Özdemir, Ö., Kaya, M.O.: Flapwise bending vibration analysis of a rotating tapered cantilevered Bernoulli–Euler beam by differential transform method. J. Sound Vib. **289**, 413–420 (2006)
19. Sato, K.: Transverse vibrations of linearly tapered beams with ends restrained elastically against rotation subjected to axial force. Int. J. Mech. Sci. **22**, 109–115 (1980)
20. Storti, D., Aboelnaga, Y.: Bending vibration of a class of rotating beams with hypergeometric solutions. ASME J. Appl. Mech. **54**, 311–314 (1987)
21. Swaminathan, M., Rao, J.S.: Vibrations of rotating, pretwisted and tapered blades. Mech. Mach. Theory **12**, 331–337 (1977)
22. To, C.W.S.: Higher order tapered beam finite elements for vibration analysis. J. Sound Vib. **63**, 33–50 (1979)
23. Williams, F.W., Banerjee, J.R.: Flexural vibration of axially loaded beams with linear or parabolic taper. J. Sound Vib. **99**, 121–138 (1985)